Microstructure and Broadband Dielectric Properties of Zn_2SiO_4 Ceramics with Nano-sized TiO_2 Addition

Zhangzhao Weng[1, 5], Chunxiao Song[1], Zhaoxian Xiong[1], Hao Xue[1,*], Wenfeng Sun[2], Yan Zhang[2], Bin Yang[2, 3**], Michael J Reece[4] & Haixue Yan[4]

[1]Department of Materials Science and Engineering, Xiamen University, Xiamen 361005, China

[2]Department of Physics, Beijing Key Lab of Metamaterials and Devices, and Key Laboratory of Terahertz Optoelectronics, Ministry of Education, Beijing Advanced Innovation Center for Imaging Technology, Capital Normal University, Beijing 100048, People's Republic of China

.[3]Department of Electronic and Electrical Engineering, University of Chester, Chester, CH2 4NU, United Kingdom

[4]School of Engineering and Material Sciences, Queen Mary, University of London, London, E1 4NS, United Kingdom

[5]China Electronic Product Reliability and Environmental Testing Research Institute, No.110 Dongguanzhuang Road, Guangzhou 510610, China

Abstract

Zn_2SiO_4 ceramics with nano-sized TiO_2 addition (ZST) were synthesized by conventional solid state method. The association between the new composite's microstructures and dielectric properties reveals that reduced pores, increased density and average grain sizes with increasing sintering temperatures, have contributed to the increased permittivities at kHz and microwave bands; the decrease of the permittivities at 1275 ^{0}C is due to the form of twin planes. At the terahertz band, the competition of generating oxygen vacancies and forming them into twin crystallographic shear planes dominates the change of permittivities: the crystallographic shear planes decrease the permittivity at the sintering temperature 1225^{0}C and 1250^{0}C, and the high-rate generation of oxygen vacancies at 1275 ^{0}C increases the permittivities. The ZST ceramics demonstrate stable permittivity and low dielectric losses ($<10^{-3}$ from 10 kHz to microwave band; and $< 10^{-2}$ at THz range); and the temperature coefficient of resonant frequency is optimized to close zero. These advanced dielectric properties and low sintering temperature (<1300^{0}C) provide the ZST ceramics great potential in designing microwave and THz devices.

Keywords: W**illemite, Broadband dielectric properties, Microwave ceramics, Terahertz (THz).**

1. Introduction

Microwave technologies have recently been developed for widespread applications, and dielectric materials play a crucial role in their performances. For example, dielectric materials can miniaturize the size of components (transmitter, receiver, filters) inside of mobile phones, base stations, microwave integrated circuits and ultrahigh-speed wireless LAN [1-6]. Great attention had been paid to materials like (Zr, Sn) TiO_4 [7, 8], $BaTi_4O_9$ [9, 10] and Ba ($Zn_{1/3}$, $Nb_{2/3}$) O_3 [11] as they have suitable permittivity values, high quality factors and near-zero temperature coefficient of resonant frequency, which are crucial technical parameters for high performance microwave system and devices.

In recent year, the technologies have been expanded to millimeter wavelength and terahertz (THz) bands due to the shortage of available frequency regions [12]. THz waves, an electromagnetic wavelength from 0.1 THz to 10 THz, are now applied in many practical fields such as passive body scanning [13], fingerprinting and chemical identification [14], and are highly potential for next generation communication system [15]. Various kinds of materials have been explored to make devices operating at THz frequencies. For example, $LiNbO_3$ and $LiTaO_3$ single crystals are reported as a high field intensity THz source materials [16, 17]; $Bi(Sc_{1/3}Mo_{2/3})O_4$ ceramics, attracted much attention as photocatalysis materials, have been reported having a relatively stable permittivity (~24.4), linearly but rapidly increased loss tangent from 0.004 at 0.1 THz to 0.3 at 1.4 THz [18]; low-temperature co-fired ceramics (LTCC), for example MgO–ZnO–TiO_2 ceramics and $CaTiO_3$ doped MgO–ZnO–TiO_2 ceramics, have shown low dielectric loss tangent (~0.02) at 0.3 THz [19], which have been used as packaging

materials for sub-THz antenna front-end [20, 21].

For substrate materials in microwave and THz applications, the dielectrics should have stable permittivities (ε_r), low dielectric losses and near-zero temperature coefficient of resonant frequency (τ_f). In telecommunication technologies, Zn_2SiO_4 ceramics have been a promising choice due to their low permittivity, high quality factor (Q) and adjustable τ_f values to near zero. Its low permittivity is attributed to the existence of a high ratio of covalent bonding. It is known that Zn_2SiO_4 has three different kinds of crystal structures, α-, β- and γ-Zn_2SiO_4 [22]. The α-Zn_2SiO_4 phase (willemite) is the only stable phase, the β-Zn_2SiO_4 and γ-Zn_2SiO_4 phases are metastable and they are easily transformed to the α-phase at high temperature [23]. α-Zn_2SiO_4 has trigonal phase with rhombohedral structure consisting of an isolated $[SiO_4]^{4-}$ tetrahedrons and $[ZnO_4]^{6-}$ tetrahedrons connected by shared oxygen atoms [24, 25]. This high ratio of covalent bonding produces low permittivity of Zn_2SiO_4 [26]. Pure Zn_2SiO_4 have high Q*f value, more than 28,742 GHz (at 15.7 GHz) [27]. Another important property of Zn_2SiO_4 is near zero value of τ_f, which can prevent the shift of resonant frequency with temperature change to offer performance stability and reliability at different environment [28]. The τ_f values of TiO_2 and Zn_2SiO_4 are ~+450 ppm/^{0}C and -61ppm/^{0}C respectively, and the τ_f of Zn_2SiO_4 with TiO_2 addition can be adjusted to near zero when the amount of TiO_2 is ~10-12 wt% [29]. However, the association between the new microstructures and its novel properties hasn't been systematically investigated, which is crucial for its applications.

In our work, Zn_2SiO_4 ceramics were synthesized using solid state sintering method,

and nano-sized TiO_2 powders as raw material are added in order to reach near-zero τ_f value and decrease the sintering temperature. The properties of Zn_2SiO_4 with the addition of TiO_2 powders, i.e., ZST ceramics were studied using XRD, XPS, Raman, SEM and EDS. Moreover, the dielectric properties of ZST over a broadband frequency range from 10 kHz to 2 THz were fully investigated. The association between the dielectric properties at different electromagnetic bands and their microstructures is comprehensively reported for the first time.

2. Experimental Section

Highly-purified oxide powders of ZnO, SiO_2 (both >99.99%, the West Long Chemical Corporation) were chosen as the starting materials. They were mixed according to the stoichiometric formula Zn_2SiO_4, and ball-milled for 4 h using distilled water as the medium. The mixture was dried and then calcinated at 1150^0C for 2 h. After that, the calcinated powders were ball-milled again for 4 h with 10wt% nano-sized TiO_2 (mean size ~20 nm, Evonik Degussa Corporation) additions. The mixture was granulated with an organic binder poly vinyl alcohol (PVA) and then pressed into cylindrical compacts under 200 MPa pressure. Finally the samples were sintered at 1200 ^{0}C, 1225 ^{0}C, 1250 ^{0}C and 1275 ^{0}C respectively for 5 h with a heating rate of 5 ^{0}C /min in the air. The bulk density of the sintered samples was measured by the Archimedes' method. The crystal structure and phase constitution were determined by X-ray powder diffraction analysis (XRD, Bruker-AxsD8 Diffractometer, Germany) with Cu-Kα radiation. The microstructure observations and element distribution of the sintered specimens were performed by scanning electron microscopy (SEM, Hitachi

SU70, Japan, and FEI, Inspect F, USA) and energy dispersive spectra analysis (EDS, Hitachi SU70, Japan) respectively. The grain size distribution and average grain size were determined based on 200 grains in the SEM images by Image-Pro plus software. X-ray photoelectron spectroscope (XPS, PHI Quantum 2000, USA) with X-ray source of Mg Kα was used to study the variation of titanium ion valence state and oxygen vacancies. Raman spectra were obtained from sintered specimens using a Confocal Raman Microscope (TriVista CRS557, Princeton Instruments, USA) equipped with a 532 nm laser (Crystalaser, USA) with laser power of 100mw. The dielectric properties of the samples were investigated at different frequency ranges. At low frequency, from 10 kHz to 10 MHz, the permittivity and dielectric loss tangent were measured using an impedance analyzer (4294A, Agilent, USA). In the microwave frequency range, the permittivity and $Q \times f$ values were measured in the TE_{011} mode using the Hakki and Coleman method [30]. A network analyzer (E8362B, Agilent, USA) was used to drive the measurement system. The τ_f value was evaluated in the temperature range between 20 ^{0}C and 80 ^{0}C, and then calculated by the following equation:

$$\tau_f = \frac{f_{80} - f_{20}}{f_{20} \times 60} \times 10^6 (\text{ppm}/^\circ\text{C}) \qquad (1)$$

Here f refers to the resonant frequency; subscripts of 20 and 80 refer to the testing temperature.

The dielectric properties at THz frequencies were measured using a THz-TDS (THz time-domain spectroscopy) system (from TeTechs Ltd). Thin polished plane-parallel specimens (~0.8 mm) were measured from 0.2 THz to 2 THz in transmission mode to obtain the time domain spectrum. Using the Fourier transformation function, the

corresponding amplitude and phase spectra versus frequency were determined. After that, dielectric parameters including permittivity and loss tangent in the THz region were calculated according to the information of amplitude, phase, reference spectrum and the samples' spectra.

3. Results and Discussions

3.1. Crystal Structure

The XRD patterns of the ZST ceramics sintered at various temperatures are shown in the Fig.1. For all of the samples only two phases can be observed: the Zn_2SiO_4 willemite phase and the TiO_2 rutile phase. All of the diffraction peaks can be assigned exactly to the standard card of Zn_2SiO_4 (JCPDS no.37-1485, willemite) and TiO_2 (JCPDS no.21-1276, rutile), whereas no peaks corresponding to SiO_2, ZnO, Zn_2TiO_4 or any new phase formed by the reaction with TiO_2 are observed. This suggests that a "composite" mixing effect occurs between Zn_2SiO_4 and TiO_2 instead of chemical reactions. Zn_2SiO_4 and TiO_2 contribute independently to the dielectric properties of the composite ceramics including permittivity, loss tangent and τ_f values.

3.2. Density

The bulk density of ZST ceramics is shown in Fig.2, where the density increases monotonically with the increase of the sintering temperature. Commonly to obtain dense Zn_2SiO_4 ceramics a high sintering temperature above 1340 ^{0}C would be chosen [31]; however, the sintering temperature in this work has been decreased below 1275 ^{0}C with adding of nano-sized TiO_2 particles, whose sintering temperature is ~1100 ^{0}C [5]. The addition of nano-sized TiO_2 promotes the sintering progress, so that it can

decrease the sintering temperature. All of the measured densities were greater than 96% of theoretical density when the sintering temperature is greater than 1225 ^{0}C, which benefits in decreasing the dielectric loss and optimizing the dielectric performance.

3.3. Morphology and Elemental Analysis

The SEM micrographs including as-sintered and fractured surfaces of the ZST ceramics are showed in Fig.3 (a)-(h), where the grains are spherical shape and faceted; the fractured surface exhibits transgranular fracture morphology. The insets of Fig.3 show the grain size distributions with the fitted results. According to the elemental distribution map of EDS analysis as shown in Fig. 4 (a), it is identified that the bigger grains are Zn_2SiO_4 and the smaller grains are TiO_2, whose average grain sizes are 1.6μm and 0.9μm respectively. Meanwhile, increasing the sintering temperature has caused the growth of grains. We denote g_s to represent the average grain size and it is statistically listed in Table 1. From Fig.3 (a) and (b), the sample sintered at 1200^{0}C has pores existed at the boundaries. During the sintering process, some parts of the pores on the boundaries can disappear. From the fractured surface as shown in Fig.3 (h), the grains grow bigger and more completely at 1275^{0}C, however some pores are still observed. The monotonically increased density data illustrate clearly that the sintering temperature is sufficient for complete densification of ZST ceramics, and the pores are still observable but with little influence as sintering temperature is increased.

According to the EDS data, Zn, Si, Ti and O are all detected and the chemical composition is identified in the elemental maps. In Fig.4 (a), the ZST sample sintered at 1200 ^{0}C has a homogeneous distribution of Ti elements. With increasing the sintering

temperature, the distribution of TiO_2 grains is inhomogeneous because of the aggregation of Ti element during the sintering process. A sharp boundary has been observed from SEM results as shown in Fig.4.b which could be twin crystal grains there, and this kind of structure has been observed by other researchers [32]. Ti and O elements are detected on the surface of the grains, as shown in the EDS data (Fig.4b.III insert). It has been reported that TiO_2 is not very stable in valence state and Ti^{4+} tends to transform into Ti^{3+} owing to the appearance of oxygen vacancies during high temperature sintering. This mechanism could be expressed as following equation [33]:

$$O^x_O + Ti^{4+} \leftrightharpoons V_O^{\cdot\cdot} + e' + \frac{1}{2}O_2 + Ti^{3+} \qquad (2)$$

In literature [34], XPS results of Ti 2p can provide a strong and direct evidence of Ti reduction, which has been shown in TiO_2-based samples. However, due to the low concentration of Ti ion in this work, the signal-to-noise of XPS peak of Ti ion is too low to be identified. XPS is highly sensitive to the oxidation state of the elements, therefore, XPS of the O 1s peak is taken to assist the explanation of Ti ion reduction. Fig.5 displays the XPS results of the binding energy of O 1s, where the intensity peak at 531.87 eV is observed for the sample sintered at 1200^0C, and the peak is significantly red-shifted for the sample sintered at 1275^0C before slightly blue-shifted for the samples sintered at the temperature 1225^0C and 1250^0C. The blue shift is mainly caused by the formation of crystallographic shear planes due to the aggregation of oxygen vacancies; the following red shift at higher sintering temperature is caused by higher rate of producing oxygen vacancies than that of eliminating oxygen vacancies by the shear plane processing [32, 34]. This red shift of O 1s peak has demonstrated the reduction of Ti ion.

3.4. Raman Spectrum

The Raman spectra of ZST ceramics at room temperature are shown in Fig.6. The Raman peak at ~240cm^{-1} is associated with a second order phonon mode of TiO_2, and

the peak at ~450cm^{-1} originates from the planar O-O vibration mode and the peak at ~613cm^{-1} is related to the Ti-O stretching vibration respectively [34]. The peaks induced by the existence of Zn_2SiO_4 are not as strong as TiO_2, because of the high ratio of covalent bonding in Zn_2SiO_4 and the symmetry of the SiO_4 and ZnO_4 tetrahedron leads to high structural stability, which make their vibrations harder. The peaks attributed to the vibration of ZnO_4 group should appear at the range from 300 to 700 cm^{-1} [35], however they are covered by TiO_2's Raman peaks at ~450cm^{-1} and ~615cm^{-1}. The peaks in the region between 800- 1000 cm^{-1} are assigned to the stretching vibrations of the SiO_4 group [36]. The Raman spectra are quite similar for the ZST ceramics sintered at 1200^{0}C and 1250 ^{0}C, however, the intensity of the peaks for the sample sintered at 1275 ^{0}C is significantly lower than that of other samples. With the assistant of SEM and EDS results in Fig3 (d) and Fig.4 (b), the lower Raman intensity peak can be possibly attributed to the non-uniformed distribution of TiO_2 and the changes of composition in small local area at higher sintering temperature, which is related to the Ti ion reduction supported by XPS results in Fig 5.

3.5. Dielectric Properties.

The addition of nano-sized TiO_2 can adjust the dielectric properties of Zn_2SiO_4 ceramics according to the well-known empirical model for multiphase ceramics [37, 38]:

$$\ln\varepsilon = x_1\ln\varepsilon_1 + x_2\ln\varepsilon_2 \qquad (3)$$

$$\tan\delta = x_1\tan\delta_1 + x_2\tan\delta_2 \qquad (4)$$

$$\tau_f = x_1\tau_{f1} + x_2\tau_{f2} \quad (5)$$

Here *x* is the volume fraction, and the subscripts 1 and 2 refer to different phases of Zn_2SiO_4 and TiO_2. As TiO_2 has higher permittivity and loss tangent than pure Zn_2SiO_4, the addition of TiO_2 can increase the permittivity and loss tangent of ZST composite ceramics.

The dielectric properties from 10 kHz to 2 THz for ZST ceramics at different sintering temperatures are shown in Fig.7. The permittivity values are generally flat in the lower frequency range; however, they are increased with increasing the temperature, i.e., from 9.0 at 1200 ^{0}C to 10.8 at 1250 ^{0}C and then slightly decreased to 10.5 at 1275 ^{0}C. Microwave dielectric properties of ZST ceramics have a similar changing tendency to the lower frequency range. In Fig. 7 (b) the permittivity values of ZST ceramics are increased from 8.69 to 9.11 at 1250 ^{0}C and then decreased slightly to 8.8 at 1275 ^{0}C. Increasing the permittivity with increasing temperature is attributed to the increased densification processing and the growth of grains of the ceramics. The growth of grains can improve the ratio of grain volume to grain boundaries, and then increase the permittivity. When the sintering temperature is higher than 1250 ^{0}C, the density of ZST ceramics has no further improvement as shown in Fig.2. Therefore, the contribution of the densification is less important to the permittivity values. Alternatively, TiO_2 crystallographic shear planes are observed in Fig. 5 and they represent the reduction of oxygen vacancies concentration, which can decrease the contribution of the oxygen-vacancy-related dipoles and result in decreased permittivity. The permittivity values at microwave frequencies are slightly smaller than those at lower frequencies. The

permittivity of the sample sintered at 1250 ^{0}C is 10.8 at 10 kHz and 9.11 at 12.45 GHz. This decrease is attributed from the weakening of the dipolar polarization contribution with increasing frequency [19].

The dielectric loss tangent of ZST ceramics is stable and less than 1×10^{-3} from 10 kHz to 10 MHz, the reason is there are no secondary phases (like ZnO or SiO_2) in the composite [31]. The loss tangent of ZST at microwave frequency range is showed in Fig. 7 (c) and listed in Table.2. The dielectric loss is lower than 1×10^{-3} as well and is decreased with the sintering temperature monotonically. In general, the large grain size of well-sintered ceramics results in low dielectric loss, therefore, densification and the growth of grains of ZST ceramics are the main contributors to low loss properties.

The temperature coefficient of resonant frequency τ_f values of ZST ceramics varies from -61 ppm/^{0}C of pure Zn_2SiO_4 ceramics to nearly zero by the addition of TiO_2 (τ_f = +450 ppm/^{0}C) as presented in Table.2. The components Zn_2SiO_4 and TiO_2 are mixed but they keep their independent phases in ZST ceramics according to the XRD patterns in Fig.1. The τ_f values are adjusted to -11.29 ppm/^{0}C according to the equation (5), which is higher than the measured τ_f value due to the uniformity of the mixture and pores between the grains of two phases.

In the THz frequency range, from 0.2 THz to 2 THz, the dielectric properties of ZST ceramics have opposite changing tendency compared with that in the kHz and microwave bands. The permittivity firstly is decreased from 9.0 at 1200 ^{0}C to 6.8 at 1250 ^{0}C, and then increased to 8.5 at 1275 ^{0}C. At microwave frequencies, the porosity, density and grain size are dominant factors in determining the permittivities, while

defects related dipoles and lattice vibrations are more important in the THz band. In our research, the sintering temperatures are from 1200 ^{0}C to 1275 ^{0}C, which are much higher than the sintering temperature of TiO_2, typically 1100 ^{0}C. This high temperature can induce the formation of oxygen vacancies as Ti^{4+} tends to transform into Ti^{3+} at high temperature. It can also lead to the formation of crystallographic shear planes and decrease amounts of oxygen vacancies at the same time as reported in [34]. From 1200 ^{0}C to 1250 ^{0}C, the rate of eliminating oxygen vacancies exceeds that of producing oxygen vacancies, the deceased amount of oxygen vacancies reduces the permittivity. At higher temperature, the amount of oxygen vacancies is increased again, so the permittivities are increased. From the Raman results in the insert of Fig.6, the position of planar O-O vibration peak at ~450cm^{-1} and Ti-O stretching vibration peak at ~613cm^{-1} are blue-shifted initially and then red-shifted. These shifts are due to the lattice level vibrations and they cause the change of permittivities, particularly at THz range as shown in Fig 7. As the sintering temperature increases, the blue-shift indicates the harder freedom to allow lattices' vibrations in the stabler structures, therefore, the permittivity is reduced. The red-shift at higher sintering temperatures is caused from inharmonic behavior of the crystals, which produces an increase of permittivity.

4. Conclusions

Zn_2SiO_4 ceramics with 10.wt% nano-sized TiO_2 addition (ZST) were synthesized by conventional solid state method at five different temperatures, i.e., 1200 ^{0}C, 1225 ^{0}C, 1250 ^{0}C and 1275 ^{0}C. The TiO_2 addition was able to adjust the τ_f value close to zero (~-9.6 ppm/^{0}C), and also decreased the sintering temperature below 1300 ^{0}C. The low

sintering temperature didn't create microstructural disadvantages and the samples maintained their high densities (>96%). The SEM micrographs and EDS analysis showed that the reduced pores and the grown grains have produced the increase of permittivities at kHz and microwave bands, and the formed twin planes at 1275^0C caused the downward permittivities. The revolution of oxygen vacancies takes the decisive role to the permittivities at THz band: forming oxygen vacancies into shear planes causes the decrease of permittivites at 1225 ^{0}C and 1250 ^{0}C, while increased number of oxygen vacancies at 1275 ^{0}C upturns the permittivites again. The ZST ceramics' stable permittivity and low dielectric losses over a wide range of electromagnetic spectrum make them suitable substrate materials for microwave and THz applications.

Acknowledgement

This work was financially supported by the Natural Science Foundation of Fujian Province of China (No. 2017J01098) and scholarship from Xiamen University for supporting academic visiting abroad.

References

[1]P.Kumari, P.Tripathi, B.Sahu, S.P.Singh, D.Kumar., Four-element composite triangular dielectric resonator antenna using Li_2O-1.94MgO-0.02Al_2O_3-P_2O_5 ceramic for wideband applications. J. Electron. Mater., 47 (2018) 5218-5228.

[2]L.Ren, X.Luo, H.Zhou., The tape casting process for manufacturing low-temperature co-fired ceramic green sheets: A review. J. Am. Ceram. Soc., 101 (2018) 3874-3889.

[3]M.C.Kang, G.Byun, H.Choo. Design of a miniaturized dual-band antenna for improved directivity using a dielectric-loaded cavity. Micro. Opt. Techn. Let., 58 (2016) 1591-1595.

[4]G.Subramanyam, M.W.Cole, N.X.Sun, T.S.Kalkur, N.M.Sbrockey, G.S.Tompa, X.Guo, C.Chen, S.P.Alpay, G.A.Rossetti, J.K.Daya, L.Chen, D.G.Schlom., Challenges and opportunities for multi-functional oxide thin films for voltage tunable radio frequency/microwave components. J. Appl. Phys., 114(2013) 191301.

[5]Z.Weng, C Wu, Z.Xiong, Y.Feng, H.AminiRastabi, C.Song, H.Xue., Low temperature sintering and microwave dielectric properties of TiO_2 ceramics. J. Eur. Ceram. Soc. 37(2017) 4667-4672.

[6]N.Akhtar, H.M.Rafique, S.Atiq, S.Aslam, A.Razaq, M.Saleem., Ni doped ZrTiO4 ceramics for dielectric resonator applications. J. Mater. Sci.: Mater. Electron. 29 (2018) 13220–13228.

[7]D.Pamu, G.L N.Rao, K. C.J. Raju., Enhanced microwave dielectric properties of ($Zr_{0.8}$, $Sn_{0.2}$) TiO_4 ceramics with the addition of its own nanoparticles. J. Am. Ceram.

Soc., 95 (2012) 126–132 (2012).

[8]Y.S Ho, T.S Chen, W.D Yang., The effect of tin precursors on the formation of $Zr_{0.8}Sn_{0.2}TiO_4$ nano-powder by sol gel process. J. Sol-Gel Sci. Technol., 53 (2010) 613–618.

[9]H.Ren, T.Xie, M.Dang, S.Jiang, H.Lin, L.Luo., Sintering mechanism and microwave dielectric properties of $BaTi_4O_9$-BBZ composite for LTCC technology. Ceram. Int., 43 (2017) 12863–12869.

[10]H. Ren, T. Xie, M. Dang, S. Jiang, H. Lin, L. Luo., The influence of BBZ glass on phase evolution, sintering behavior and dielectric properties of $BaTi_4O_9$ ceramics. J. Mater. Sci.: Mater. Electron. 28 (2017) 19090–19097.

[11]R.I. Scott, M. Thomas and C. Hampson., Development of low cost, high performance Ba ($Zn_{1/3}Nb_{2/3}O_3$) based materials for microwave resonator applications. J. Eur. Ceram. Soc., 23 (2003) 2467–2471.

[12]H.Ohsato, T.Tsunooka, A.Kan, et al., Microwave-millimeter wave dielectric materials. Key Engineering Materials, 269 (2004) 195-198.

[13]R.Knipper, A.Brahm, E.Heinz, T. May, G.Notni, H.G Meyer, A. Tunnermann, and J. Popp., THz absorption in fabric and its impact on body scanning for security application. IEEE Trans on THz Sci. Techn., 5 (2015) 999-1004.

[14]A.I.McIntosh, B.Yang, S.M.Goldup, M.Watkinson and R.S.Donnan., Terahertz spectroscopy: a powerful new tool for the chemical sciences?.Chem. Soc. Rev. 41 (2012) 2072–2082.

[15]T.Kurner and S.Priebe., Towards THz communications – status in research,

standardization and regulation. J.Infrared Mill.Terahz Waves 35, 53-62 (2014).

[16]H.Igawa, T.Mori, S.Kojima., Terahertz time-domain spectroscopy of congruent $LiNbO_3$ and $LiTaO_3$ crystals. Jpn. J. Appl. Phys. 53 (2014) 05FE01.

[17]L.Tokodi, A.Buzády, J.Hebling, L.Pálfalvi., Possibility of high□energy THz generation in LiTaO3. Appl. Phys. B, (2016)122:235.

[18]D.Zhou, L.Pang, D.Wang, H.H Guo, F.Yang, Z.M Qi, C. Li, B.B Jin, I. M. Reaney., Crystal structure, impedance and broadband dielectric spectra of ordered scheelite-structured $Bi(Sc_{1/3}Mo_{2/3})O_4$ ceramic. J. Eur. Ceram. Soc. 38 (2018) 1556–1561.

[19]S.Wang, Q.Li, J.Gu, J.Han, W.Zhang., Dielectric properties of MgO–ZnO–TiO_2-based ceramics at 1 MHz and THz frequencies. J. Mater. Sci., 52 (2017) 9335–9343.

[20]T.Tajima, H.J.Song, K.Ajito, M.Yaita, N.Kukutsu., 300-GHz step-profiled corrugated horn antennas integrated in LTCC. IEEE transactions on antennas and propagation, 62 (2014) 5437-5444.

[21]T.Tajima, H.J.Song, M.Yaita., Compact THz LTCC receiver module for 300 GHz wireless communications. IEEE microwave and wireless components letters, 26 (2016) 291-293.

[22]M.Takesue, H.Hayashi, R.L.S.Jr., Thermal and chemical methods for producing zinc silicate (willemite): A review. Prog. Cryst. Growth Charact. Mater. 55 (2009) 98-124.

[23]R.Ye, G.Jia, D.Deng, Y.Hua, Z.Cui, S.Zhao, L.Huang, H.Wang, C.Li, S.Xu., Controllable synthesis and tunable colors of α- and β-$Zn_2SiO_4:Mn^{2+}$ nanocrystals for UV and blue chip excited white LEDs. J. Phys. Chem. C 115 (2011) 10851–10858.

[24]K.H.Klaska, J.C.Eck and D.Poh., New Investigation of Willemite. Acta Cryst. B34 (1978) 3324-3325.

[25]R.F.Samigullina, A.P.Tyutyunnik, I.N.Gracheva, G.I.Krasnenko, N.A.Zaitseva, T.A.Onufrieva., Hydrothermal synthesis of a-Zn_2SiO_4:V phosphor, determination of oxidation states and structural localization of vanadium ions. Mater. Res. Bull. 87 (2017) 27-33.

[26]Z.Weng, R.Guan, Z.Xiong., Effects of the ZBS addition on the sintering behavior and microwave dielectric properties of $0.95Zn_2SiO_4$-$0.05CaTiO_3$ ceramics. J. Alloys Comp. 695 (2017) 3517-3521.

[27]Z.Weng, H.AminiRastabi, Z.Xiong, H.Xue., Effects of the Bi_2O_3-SiO_2 addition on the sintering behavior and microwave dielectric properties of $Zn_{1.8}SiO_{3.8}$ ceramics. J. Alloys Comp. 725 (2017) 1063-1068.

[28]H.Jantunen, A.Uusimaki, R.Rautioaho, S.Leppavuori., Temperature coefficient of microwave resonance frequency of a low-temperature cofired ceramic (LTCC) system. J. Am. Ceram. Soc., 85 (2002) 697–99.

[29]Y Guo, H Ohsato and K.Kakimoto., Characterization and dielectric behavior of willemite and TiO_2-doped willemite ceramics at millimeter-wave frequency. J. Eur. Ceram. Soc. 26 (2006) 1827–30.

[30]B.W.Hakki, P.D.Coleman., A dielectric resonator method of measuring inductive capacities in the millimeter range. IRE Trans on Microwave Theory & Techniques, 8 (2002) 402-410.

[31]W.C.Tsai, K.C.Chiu, Y.X.Nian, Y.C.Liou., Significant improvement of the

microwave dielectric loss of $Zn_{1.95}M_{0.05}SiO_4$ ceramics (M = Zn, Mg, Ni, and Co) prepared by reaction-sintering process. J. Mater. Sci.: Mater. Electron, 28 (2017) 14258–14263.

[32]J.V.Landuyt, R.Gevers and S.Amelinckx., Electron microscopic study of twins, anti-phase boundaries, and dislocations in thin films of rutile. Phys. Stat. Sol. 7, (1964) 307-329.

[33]Z.Xiong, B.Tang, Z.Fang, C.Yang, S.Zhang., Effects of $(Cr_{0.5}Ta_{0.5})^{4+}$ on structure and microwave dielectric properties of $Ca_{0.61}Nd_{0.26}TiO_3$ ceramics. Ceram. Int., 44 (2018) 7771-7779.

[34]C.Yu, Y.Zeng, B.Yang, R.Donnan, J.Huang, Z.Xiong, A.Mahajan, B.Shi, H.Ye, R.Binions, N.V.Tarakina, M.J Reece and HX.Yan., Titanium dioxide engineered for near-dispersionless high terahertz permittivity and ultra-low-loss. Sci. Rep., 7 (2017) 6639-6647.

[35]B.C.Babu, B.V.Rao, M.Ravi, S.Babu., Structural, microstructural, optical, and dielectric properties of Mn^{2+}:Willemite Zn_2SiO_4 nanocomposites obtained by a sol-gel method. J. Mol. Struct., 1127 (2017) 6-14.

[36]K.Omri, A.Alyamani, L.El Mir., Photoluminescence and cathodeluminescence of Mn doped zinc silicate nanophosphors for green and yellow field emissions displays. Appl. Phys. A-Mater., 124 (2018) 215.

[37]S.Keshri, S.S.Rajput, Investigation on low loss (1–x) $Mg_{0.95}Co_{0.05}TiO_{3-(x)}$ $Ca_{0.6}La_{0.8/3}TiO_3$ composite series for achieving a nearly zero temperature coefficient of resonant frequency. Ceram. Int. 40(2014)4257–4266

[38]M.Dong, Z.Yue, H.Zhuang, et al. Microstructure and microwave dielectric properties of TiO_2-doped Zn_2SiO_4 ceramics synthesized through the Sol–Gel process. J. Am. Ceram. Soc. 91 (2008) 3981-3985.

Table 1 Average grain size of the ZST samples and its two main components

Ts/℃	ZST (g_s/μm)	TiO_2 (g_s/μm)	Zn_2SiO_4 (g_s/μm)
1200	1.4±0.6	0.9±0.3	1.6±0.5
1225	1.8±0.6	1.1±0.3	1.8±0.5
1250	2.1±0.8	1.5±0.3	1.9±0.5
1275	2.7±1.3	1.9±0.7	3.1±1.4

Table 2 Dielectric parameters of ZST ceramics sintered at different temperatures in microwave frequency range.

Ts/□	Testing frequency (GHz)	Permittivity	Q*f(GHz)	Loss tangent	T_f (ppm/℃)
1200	13.59	8.69	16171	0.000840	-9
1225	13.49	8.79	23929	0.000564	-2.4
1250	12.45	9.11	27873	0.000447	-5.7
1275	13.75	8.8	37902	0.000363	-9.6

Fig.1

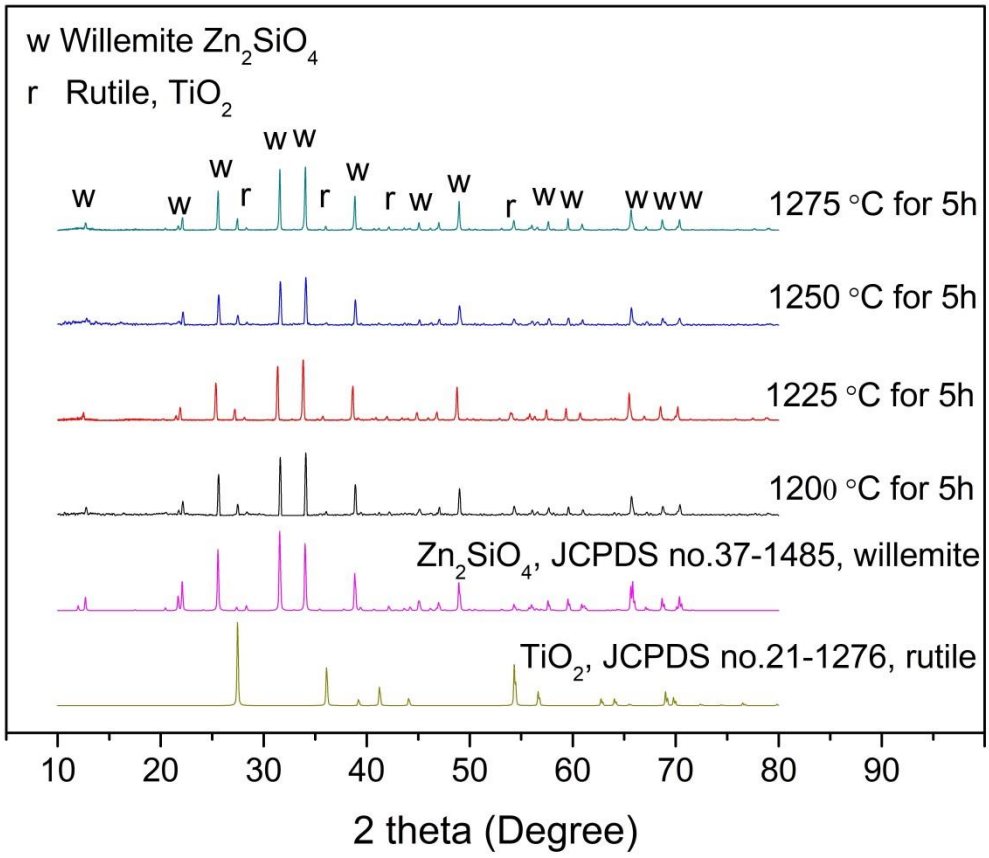

Fig.1 XRD patterns of ZST ceramics sintered at various temperatures.

Fig.2

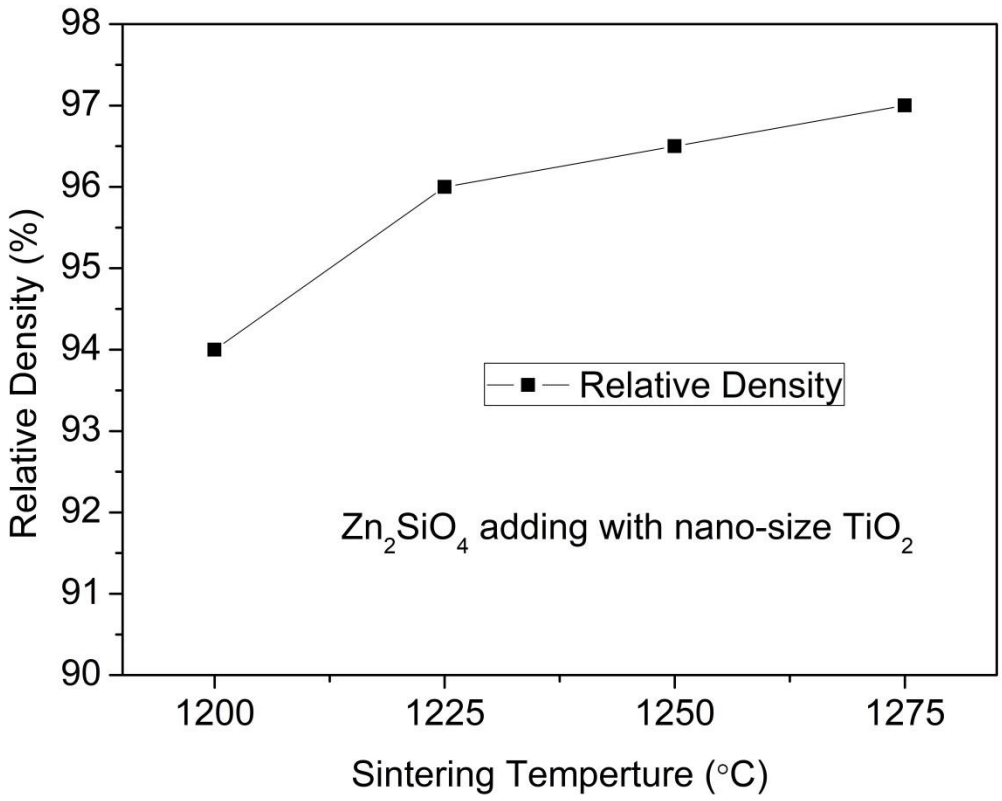

Fig.2 Variations of relative density value for ZST ceramics.

Fig.3

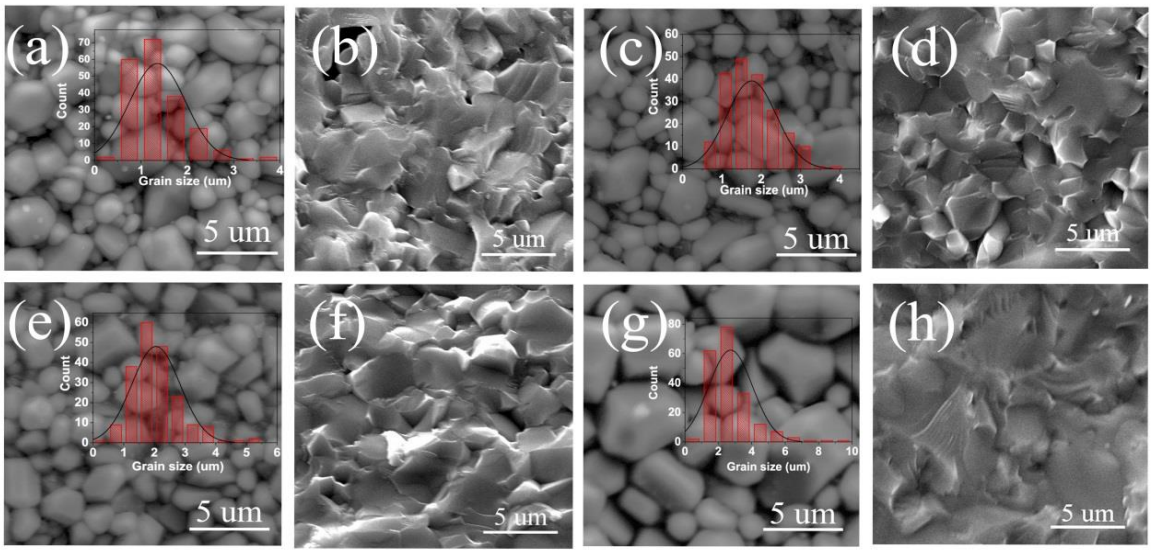

Fig.3 SEM of ZST ceramics (a) sintered at 1200 °C as-sintered surface (b) sintered at 1200 °C fractured surface (c) sintered at 1225 °C as-sintered surface (d) sintered at 1225 °C fractured surface (e) sintered at 1250 °C as-sintered surface (f) sintered at 1250 °C fractured surface (g) sintered at 1275 °C as-sintered surface (h) sintered at 1275 °C fractured surface. The insets show the calculated grain size distribution.

Fig.4

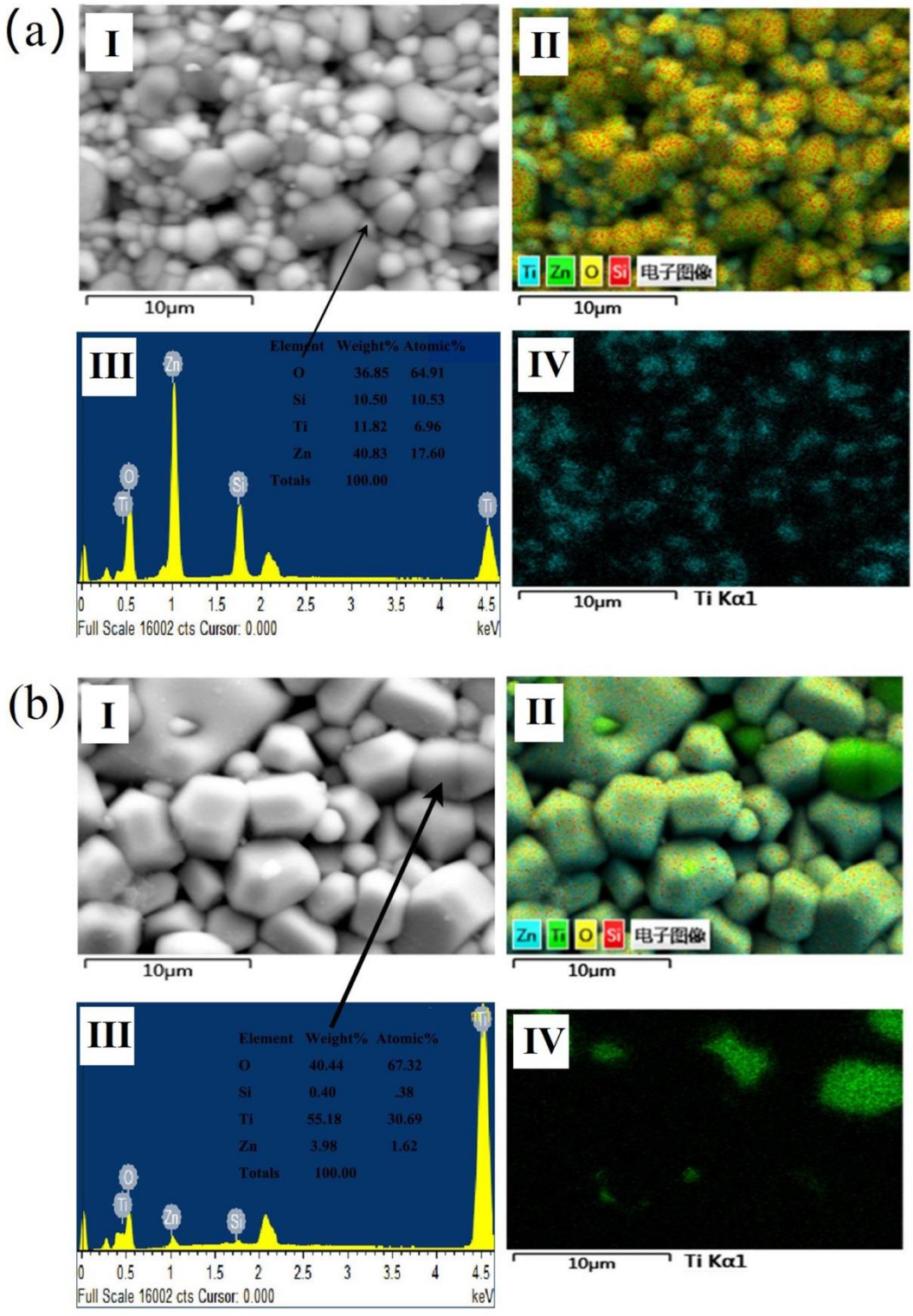

Fig.4 EDS analysis of ZST ceramic sintered (a) at 1200 °C (b) at 1275 °C for 5h.

Fig.5

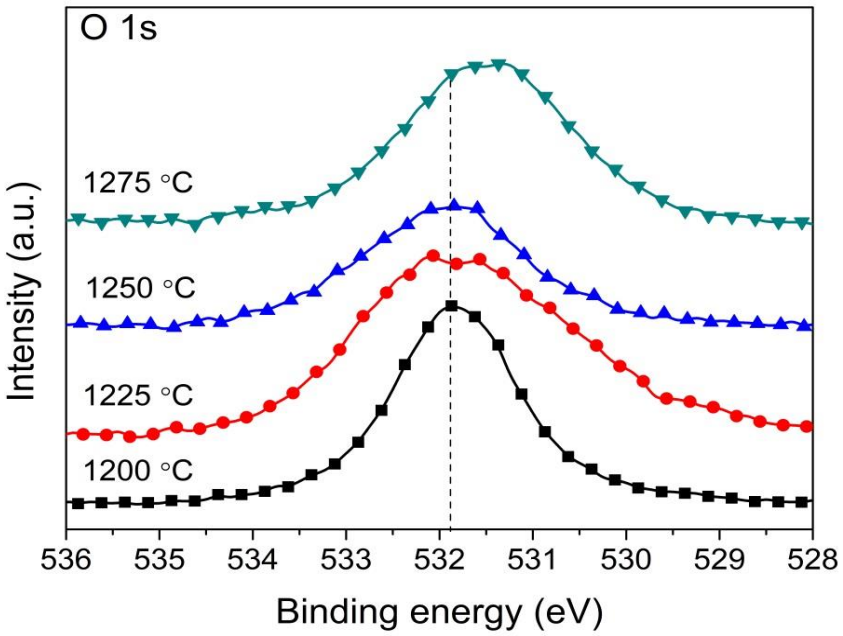

Fig.5 XPS O 1s peaks of the ZST samples sintered at different temperatures.

Fig.6

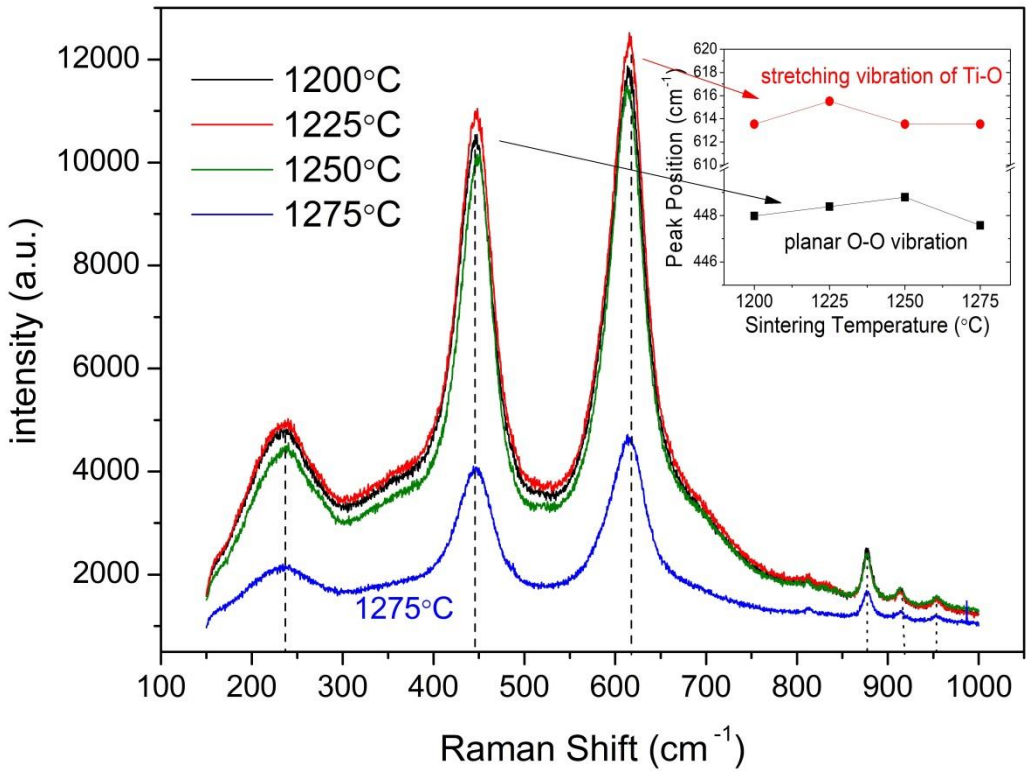

Fig.6 Raman spectra of ZST sintered at various temperatures and peak positions of Ti-O and O-O vibrations.

Fig.7

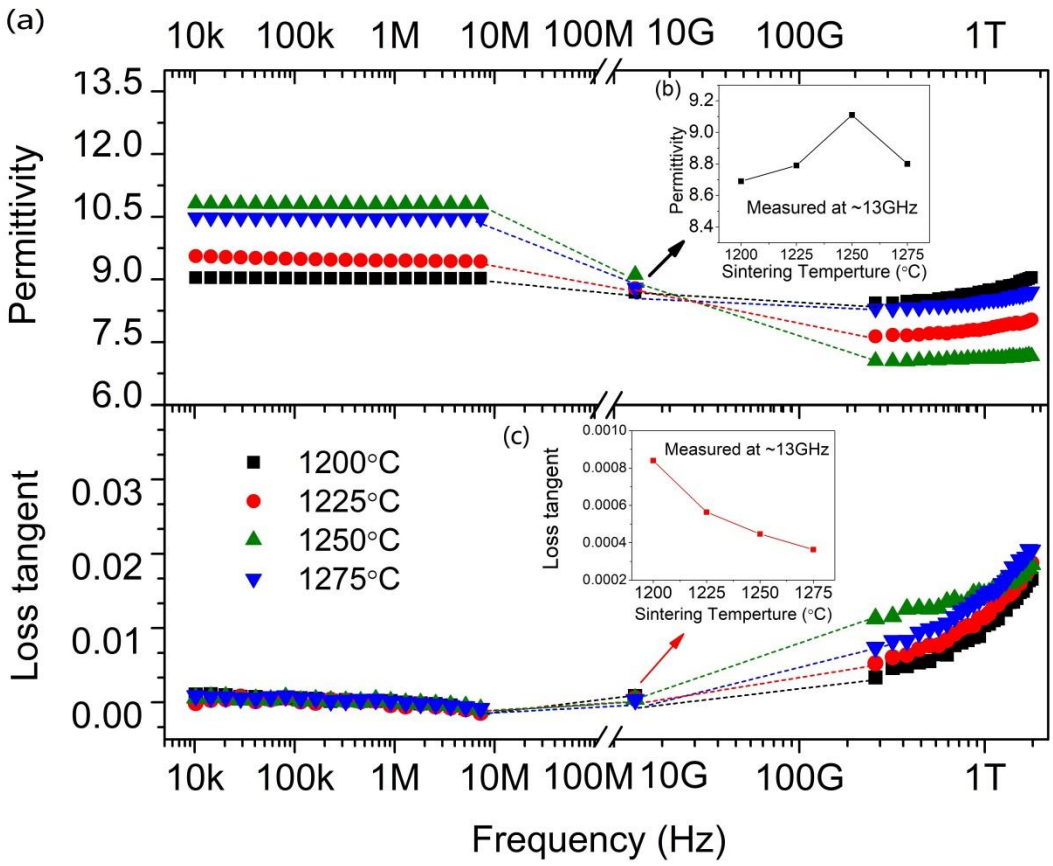

Fig.7 a) measured dielectric permittivity and loss tangent of the ZST ceramics sintered at different temperatures over a wide range of frequencies (10k-2THz); (b) the variations of the permittivity with sintering temperature at microwave frequency; (c) the variations of loss tangent with sintering temperature at microwave frequency.